IMPLEMENTATION OF HIGH-RESOLUTION SCHEMES IN FINITE-VOLUME METHODS FOR STEADY VISCOELASTIC FLOWS

MANUEL A. ALVES[1], FERNANDO T. PINHO[2], PAULO J. OLIVEIRA[3]

[1]Dept. Eng. Química, CEFT, Fac. de Engenharia, Univ. Porto, Rua dos Bragas, 4050-123 Porto,Portugal,mmalves@fe.up.pt
[2]Centro de Estudos de Fenómenos de Transporte,DEMEGI, Univ. Porto, R. Bragas, 4050-123 Porto,Portugal,fpinho@fe.up.pt
[3]Dept. Eng. Electromecânica, Univ. Beira Interior, Rua Marquês D'Ávila e Bolama, 6200 Covilhã,Portugal,pjpo@ubi.pt

ABSTRACT

The MINMOD high-resolution convective scheme was implemented in a finite-volume code operating in a general curvilinear co-ordinate system by adopting the normalised variable and space formulation of Darwish and Moukalled [1]. Predictions of the flow of UCM fluids in the 4:1 plane contraction and around a planar cylinder in a channel were used to assess the improvements in accuracy and stability of the scheme. For the contraction flow the asymptotic results for the velocity and stresses near the re-entrant corner are found to be in good agreement with Hinch's analysis [2] and the drag forces on the cylinder are in excellent agreement with those of Fan et al [3].

KEYWORDS: HIGH-RESOLUTION SCHEME, UCM, PLANAR CONTRACTION, CYLINDER FLOW.

INTRODUCTION

Accurate predictions require discretization schemes for convection of at least second order, but that is not sufficient to ensure a stable method [4]. To impart stability to higher-order discretization schemes in the finite-volume formulation (FVM), adequate convection boundedness criteria must be adopted [5]. That leads to the so-called high-resolution schemes, one of which, the MINMOD scheme, is implemented and tested in this work.

Two of the most frequently used benchmark flows for viscoelasticity are the flow in a 4:1 planar sudden contraction and the 2-D flow around a cylinder in a channel [6]. However, truly accurate and grid-independent results for these cases are not firmly established as authors do not usually present a thorough study of the order of convergence of the methods and an assessment of the uncertainties. Such undertaking requires the use of meshes finer than usual, which becomes very expensive for the finite-element methods that are in common use [7].

We present results and quantify the uncertainties of FV predictions of flows of UCM fluids in the 4:1 sudden contraction and around a bounded cylinder. The calculations were carried out with a high-resolution scheme in various meshes to allow the application of Richardson extrapolation to the limit, for error estimation.

GOVERNING EQUATIONS

The equations to be solved are those of conservation of mass, linear momentum and the constitutive equation for an UCM fluid, written as follows:

$$\frac{\partial u_i}{\partial x_i} = 0 \tag{1}$$

$$\frac{\partial r u_i}{\partial t} + \frac{\partial u_j u_i}{\partial x_j} = -\frac{\partial p}{\partial x_i} + \frac{\partial t_{ij}}{\partial x_j} \tag{2}$$

$$t_{ij} + l\left(\frac{\partial t_{ij}}{\partial t} + \frac{\partial u_k t_{ij}}{\partial x_k}\right) = h\left(\frac{\partial u_i}{\partial x_j} + \frac{\partial u_j}{\partial x_i}\right) + l\left(t_{jk}\frac{\partial u_i}{\partial x_k} + t_{ik}\frac{\partial u_j}{\partial x_k}\right) \tag{3}$$

where r is the density, u_i and t_{ij} are the Cartesian components of velocity and extra stress term, p is the pressure, l is the relaxation time and h is the shear-viscosity.

NUMERICAL METHOD

Equations (1)-(3) are transformed into a general nonorthogonal co-ordinate system for easy application of the FVM method to a collocated mesh arrangement. The dependent variables remain the Cartesian velocity and stress components and pressure. To avoid stress-velocity decoupling, a special formulation was adopted for the calculation of the stress divergent term in the momentum equations. This and other details of the method are discussed in detail in Oliveira and co-workers [4,8]. We focus here on the constitutive equation and the high-resolution scheme.

The discretised form of the constitutive equation is cast in the usual FV form at a general cell P of volume V_P

$$a_{\mathrm{P}} t_{ij,\mathrm{P}} - \sum_{\mathrm{F}} a_{\mathrm{F}} t_{ij,\mathrm{F}} = S_{t_{ij}} + \frac{l_{\mathrm{P}} V_{\mathrm{P}}}{dt} t^{0}_{ij,\mathrm{P}} \tag{4}$$

where the coefficients a_{F} are composed by convection fluxes. The high-resolution scheme was applied in the deferred correction manner of Khosla and Rubin [9]: the coefficients a_{F} and a_{P} contain fluxes evaluated with the UDS and these terms are treated implicitly; the source term $S_{t_{ij}}$ contains the difference between the actual flux (with MINMOD) and the UDS flux, and is treated explicitly. It also incorporates the part of the Oldroyd derivative on the r.h.s of Eq. (3) which is evaluated with central differences.

In MINMOD, the high-resolution scheme adopted here, the stress at cell faces appearing in the convective fluxes are evaluated as $\hat{t}_{ij,f}$, defined in Eq. (5), in the context of the normalised variable and space formulation of Darwish and Moukalled [1]

$$\hat{t}_{ij,f} = \begin{cases} \dfrac{\hat{x}_f}{\hat{x}_{\mathrm{P}}}\hat{t}_{ij,\mathrm{P}} & 0 < \hat{t}_{ij,\mathrm{P}} < \hat{x}_{\mathrm{P}} \quad \text{SOU} \\ \dfrac{1-\hat{x}_f}{1-\hat{x}_{\mathrm{P}}}\hat{t}_{ij,\mathrm{P}} + \dfrac{\hat{x}_f - \hat{x}_{\mathrm{P}}}{1-\hat{x}_{\mathrm{P}}} & \hat{x}_{\mathrm{P}} < \hat{t}_{ij,\mathrm{P}} < 1 \quad \text{CDS} \\ \hat{t}_{ij,\mathrm{P}} & \text{elsewhere} \quad \text{UDS} \end{cases} \tag{5}$$

where the subscripts U and D refer to the upstream and downstream cells to cell P and x is the nonorthogonal coordinate along which the stress varies

$$\hat{t}_{ij} = \frac{t_{ij} - t_{ij,\mathrm{U}}}{t_{ij,\mathrm{D}} - t_{ij,\mathrm{U}}} \tag{6}$$

$$\hat{x}_{ij} = \frac{x_{ij} - x_{ij,\mathrm{U}}}{x_{ij,\mathrm{D}} - x_{ij,\mathrm{U}}} . \tag{7}$$

The discretised equations for each variable are solved in a sequential manner following the revised version of the SIMPLEC algorithm, as explained in [8,10], to couple pressure and velocity. The implicit solution of the linear sets of equations at each time step is obtained with a standard pre-conditioned conjugate gradient method.

4:1 PLANAR CONTRACTION FLOW

The flow domain, sketched in Fig. 1, was represented by four consecutively refined meshes. The cells were concentrated near the re-entrant corner and the upstream wall, where the stress gradients are expected to be higher. The cell size inside each block varied in geometrical progression at a constant ratio and some characteristics of the four meshes are given in Table I.

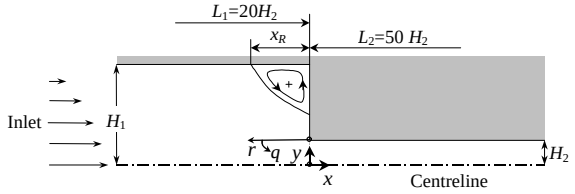

Figure 1- Schematic drawing of the sudden contraction.

Table I- Number of cells and minimum spacing

	Mesh 1	Mesh 2	Mesh 3	Mesh 4
NC	942	3598	14258	57032
$d_{\min}/H_2$	0.04	0.02	0.01	0.005

NC: number of cells; $d_{\min}$: minimum cell spacing

Mesh refinement was undertaken by doubling the number of cells along each direction in a consistent way, so that the grid spacing was approximately halved between consecutive meshes thus enabling error estimation with Richardson's extrapolation to the limit [11]. We emphasise the large number of cells in meshes 3 and 4 and the very small minimum nondimensional cell size near the re-entrant corner. These very fine meshes, in conjunction with the high-resolution scheme, allowed us to obtain very accurate solutions.

Numerical calculations of the flow of UCM fluids were performed with the MINMOD scheme at *Re*=0.01. The asymptotic behaviour of the radial velocity and normal stress components near the re-entrant corner, along direction q=p/2 (x = 0) are plotted in Figs. 2-a) and –b) together with lines of slope 5/9 and –2/3, for *De*=1. For Oldroyd-B fluids, Hinch [2] derived the following asymptotic behaviour in the vicinity of the corner

$$u_i \propto r^{5/9} \qquad t_{ij} \propto r^{-2/3} \tag{8}$$

for low values of *De*. These results express the domination of elastic stresses over solvent viscous stresses, and are also valid for a UCM fluid as well [2]. Higher values of *De* should not be considered since a significant lip vortex develops and the conditions for the applicability of Hinch's analysis are no longer valid.

The agreement is good for all velocity components and less good for the stress components calculated with the coarsest meshes. However, the predicted asymptotic stress behaviour follows Hinch's analysis quite well when fine meshes are used, a feature especially clear for t_{qq}, not shown here. The deviation next to the wall is not unexpected since numerical inaccuracies are higher there due to one-sided differences.

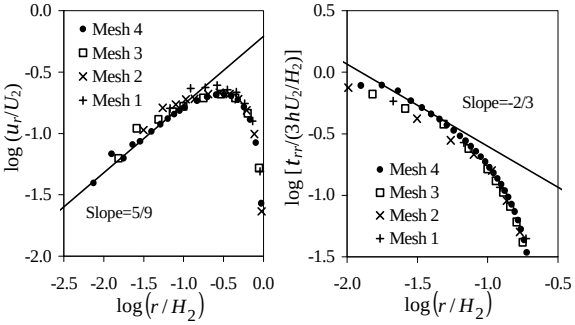

Figure 2- Asymptotic behaviour of the predicted radial velocity (a) and normal stress (b) components near the re-entrant corner, along $q = p/2$, for $De = 1$.

The calculations could be performed up to *De*=10 with mesh 3 and UDS, but with a 2nd-order upwind scheme were limited to slightly more than *De*=1. However, MINMOD has allowed us to rise *De* up to at least 5, while maintaining the second-order accuracy, as can be seen in Fig. 3. The error is estimated on the basis of extrapolated values of $X_R = x_R/H_2$ obtained from successive applications of Richardson extrapolation. Fig. 4 compares X_R obtained using UDS and MINMOD in mesh 3 and the extrapolated value based on MINMOD. Agreement between UDS and MINMOD is limited to *De*<1, with UDS predicting an increase in recirculation length at rather low values of Deborah number.

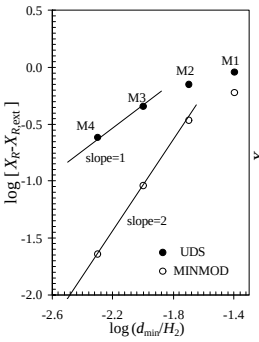

Figure 3-Estimated error on X_R, as a function of mesh refinement, at *De*=3.

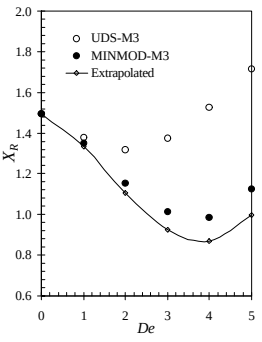

Figure 4- X_R versus *De* in mesh 3. Extrapolated values based on MINMOD.

To assess the mesh convergence we compare in Fig. 5 contours of the normalised N_1 at *De*=3. On doubling the number of cells the contours progress in a highly non-linear fashion towards asymptotic positions, typical of a second-order process: the contours from mesh 2 differ from those of meshes 3 and 4 which are very close to each other , even near the re-entrant corner.

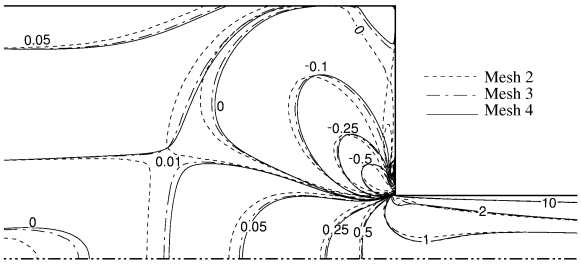

Figure 5- Distribution of $N_1/(3hU_2/H_2)$ for De=3 with MINMOD.

CYLINDER FLOW

The cylinder is located on the centreline of a channel defining a blockage ratio of 50%. The geometry requires a nonorthogonal grid and, as in the sudden contraction, several meshes were produced. The presented results are extrapolated from predictions based on meshes M60 and M120 and are compared with data from the literature [3,12]. Those meshes have 60 and 120 cells across the channel width and a total number of 17,400 and 69,600 cells, respectively. The cells are finer along the cylinder wall and in the downstream wake and the minimum cell size, normalised by the cylinder radius R, is: 0.0048 and 0.0157 along the radial and arc directions for M60; 0.00238 and 0.00785 for M120. The Deborah number is here defined as $De=lU/R$, and the results of the computations, at creeping flow conditions, are presented in two ways: the dimensionless drag coefficient C_d resulting from surface integration of stress and pressure, and profiles of stress component t_{11} along the cylinder surface and the downstream centreline.

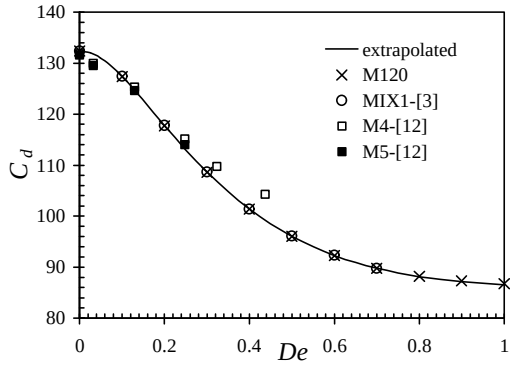

Figure 6- Comparison of predicted drag coefficients

Table II- Drag coefficient C_d on cylinder flow

De	M60	M120	Extra.	[3] Mix1
0	132.342	132.369	132.378	132.36
0.2	117.077	117.485	117.893	
	117.615	117.751	117.796	117.81
0.4	101.134	101.300	101.466	
	101.265	101.344	101.370	101.41
0.6	93.467	92.970	92.473	
	92.302	92.306	92.307	92.33
0.8	91.578	90.039	88.500	
	88.359	88.207	88.156	88.18*
1	93.063	90.268	87.473	
	87.272	86.750	86.576	

First results with UDS; second with MINMOD; * DEVSS [3]

The estimated order of convergence of the MINMOD scheme, based on C_d values on three meshes, is 1.8 at De=0.9 and 1.9 at De=0.3 . The predicted values of C_d are compared in Fig. 6 with those of Fan et al [3] and of Phan-Thien and Dou [12] obtained with finite-element and finite-volume methods, respectively, and include our extrapolated data. M4 and M5 refer to the two finest meshes of Phan-Thien and Dou [12]. Our predictions of C_d are well below those of [12], and in excellent agreement with those of Fan et al [3]. Here the differences are so small that they can only be grasped in Table II where some values are listed, together with C_d obtained using the first-order upwind scheme. The extrapolated curve is also very close to the fine mesh M120 predictions suggesting that a good degree of mesh convergence has been attained. Fan et al claim their predictions of C_d to be the most accurate in the literature on the basis that most other results show substantially higher values of C_d and, they said, that is consistent with a deterioration of accuracy. Our results support that assertion independently and suggest that the true value of C_d may be even lower.

The profiles of axial normal stress at De=0.6 in Fig. 7 show that with MINMOD mesh convergence is far superior than with UDS.

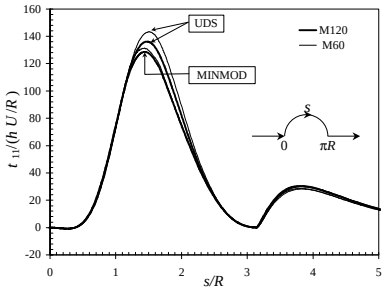

Figure 7- Profile of the axial normal stress component along the cylinder surface and the centreline at $De=0.6$.

REFERENCES

1. M. S. Darwish and F. Moukalled, *Num. Heat Transfer Part B* (1994) 26 79-96.
2. E. J. Hinch, *J. Non-Newtonian Fluid Mech.* (1993) 50 161-171.
3. Y. Fan, R. I. Tanner and N. Phan-Thien, *J. Non-Newtonian Fluid Mech.* (1999) 84 233-256
4. P. J. Oliveira and F. T. Pinho, *J. Non- Newtonian. Fluid Mech.* (1999) 88, 63-88.
5. P. H. Gaskell and A. K. C. Lau, *Int. J. Num. Meth. Fluids* (1988) 8 617-641.
6. R. A. Brown and G. H. McKinley, *J. Non- Newtonian Fluid Mech.* (1994) 52 407-413
7. S.-C. Xue, R. I. Tanner, N. Phan-Thien, *Comput. Meth. Appl. Mech. Engrg.* (1999) 180 305-331.
8. P. J. Oliveira, F. T. Pinho and G. A. Pinto, *J. Non-Newtonian Fluid Mech.* (1998) 79 1-43.
9. P. K. Khosla and S. G. Rubin, *Computers and Fluids.* (1974) 2 207-209.
10. R. I. Issa and P. J. Oliveira, *Computers and Fluids* (1994) 23 347-372.
11. J. H. Ferziger and M. Peric, *Int. J. Num. Meth. Fluids* (1996) 23 1263-1274.
12. N. Phan-Thien and H.-S. Dou, *Comput. Methods Appl. Mech. Engrg.* (1999) 180 243-266.